The Meteoritical Society

Meteoritics & Planetary Science 45, Nr 7, 1074–1092 (2010)
doi: 10.1111/j.1945-5100.2010.01090.x

Petrologic insights from the spectra of the unbrecciated eucrites: Implications for Vesta and basaltic asteroids

Rhiannon G. MAYNE[1*], Jessica M. SUNSHINE[2], Harry Y. McSWEEN[3], Timothy J. McCOY[4], Catherine M. CORRIGAN[4], and Allison GALE[5]

[1]Department of Geology, Texas Christian University, TCU Box 298830, Fort Worth, Texas 76109, USA
[2]Department of Astronomy, University of Maryland, College Park, Maryland 20742–2421, USA
[3]Department of Earth and Planetary Sciences, 1412 Circle Drive, University of Tennessee, Knoxville, Tennessee 37996–1410, USA
[4]Department of Mineral Sciences, Smithsonian Institution, National Museum of Natural History, Washington, District of Columbia 20560–0119, USA
[5]Department of Earth and Planetary Sciences, Harvard University, 20 Oxford Street, Cambridge, Massachusetts 02138, USA
[*]Corresponding author. E-mail: r.g.mayne@tcu.edu

(Received 20 July 2009; revision accepted 19 March 2010)

Abstract–We investigate the relationship between the petrology and visible–near infrared spectra of the unbrecciated eucrites and synthetic pyroxene–plagioclase mixtures to determine how spectra obtained by the Dawn mission could distinguish between several models that have been suggested for the petrogenesis of Vesta's crust (e.g., partial melting and magma ocean). Here, we study the spectra of petrologically characterized unbrecciated eucrites to establish spectral observables, which can be used to yield mineral abundances and compositions consistent with petrologic observations. No information about plagioclase could be extracted from the eucrite spectra. In contrast, pyroxene dominates the spectra of the eucrites and absorption band modeling provides a good estimate of the relative proportions of low- and high-Ca pyroxene present. Cr is a compatible element in eucrite pyroxene and is enriched in samples from primitive melts. An absorption at 0.6 μm resulting from Cr^{3+} in the pyroxene structure can be used to distinguish these primitive eucrites. The spectral differences present among the eucrites may allow Dawn to distinguish between the two main competing models proposed for the petrogenesis of Vesta (magma ocean and partial melting). These models predict different crustal structures and scales of heterogeneity, which can be observed spectrally. The formation of eucrite Allan Hills (ALH) A81001, which is primitive (Cr-rich) and relatively unmetamorphosed, is hard to explain in the magma ocean model. It could only have been formed as a quench crust. If the magma ocean model is correct, then ALHA81001-like material should be abundant on the surface of Vesta and the Vestoids.

INTRODUCTION

The upcoming Dawn mission to asteroids Vesta and Ceres has fueled renewed interest into the formation of differentiated asteroids. McCord et al. (1970) were the first to note the spectral similarities between the spectrum of Vesta and those of the igneous howardites, eucrites, and diogenites (HEDs), collectively the most abundant group of achondritic meteorites. While the spectral match between Vesta and certain HEDs was tantalizing, the proposed link suffered from lack of a mechanism to deliver meteorites from Vesta to Earth. The link was markedly strengthened with the discovery of Vesta-like asteroids (vestoids) bridging the gap between it and the 3:1 resonance with Jupiter (Binzel and Xu 1993), which is thought to be a zone for dynamically favorable meteorite delivery to Earth. If this proposed relationship is correct then the HEDs enable us to collect detailed mineralogical, petrological, and geochemical information about Vesta and the

Vestoids. This is particularly important, as Vesta is the largest intact asteroid which appears to have differentiated to form a core, mantle, and crust. In many ways, Vesta serves as an endmember in our understanding of asteroid differentiation (McCoy et al. 2006), but even the origin of this asteroid is incompletely understood (Mittlefehldt and Lindstrom 2003). The importance of differentiation and formation of basaltic crusts on asteroids was highlighted by the discovery of a basaltic surface for asteroid 1459 Magnya (Lazzaro et al. 2000; Hardersen et al. 2004) and work by Sunshine et al. (2004b) that identified the presence of high-calcium pyroxene (HCP) on several S-type asteroids, indicative of a basaltic crust.

The instrumentation on board the Dawn spacecraft was designed primarily to provide information about the surface morphology and composition of the two asteroids it will visit, with one of the science goals being to provide a geologic context for the HEDs (Russell et al. 2004, 2006). Mineralogic information will be derived primarily from the visible–infrared (VIR) spectrometer, which has detectors both in the visible (0.25–1.0 μm) and infrared (0.95–5.0 μm) wavelengths (Russell et al. 2004, 2006). To interpret the resulting spectra, we must understand the relationship between spectra and petrology. This can be achieved with combined petrologic and spectral studies of the meteorites believed to originate from Vesta.

This study examines whether the competing models for the formation of Vesta's crust can be distinguished through spectroscopy. As a first step, we examine the relationship between petrology and spectra and attempt to model the spectra to yield petrologically reasonable estimates of mineral abundances and composition. Sample selection is particularly critical as most eucrites are polymict breccias and their spectra sample a mixture of lithologies, complicating spectral interpretations. The unbrecciated eucrites are key as direct comparisons can be made between the petrologic characteristics and spectral features of the same material.

BACKGROUND

The Petrogenesis of Vesta

The two models originally proposed for the formation of Vesta are those of partial melting (Stolper 1977) and fractional crystallization (Mason 1962). Stolper (1977) observed that the noncumulate eucrites had bulk compositions that clustered around the pseduoperitectic in the silica-olivine-anorthite phase diagram. He suggested, therefore, that they are primary liquids derived from differing amounts of partial melt of an olivine-pigeonite-plagioclase-spinel-metal source. Mason (1962), on the other hand, proposed a fractional crystallization sequence, with the eucrites representing the residual liquids produced after diogenite crystallization from a chondritic source. However, neither model can completely explain the formation of the HEDs. Partial melting models are unable to match the siderophile element abundances of the eucrites (Mittlefehldt and Lindstrom 2003). Partial melting would predict a relatively constant W value due to metal buffering in the source region and a La value that would vary depending on the degree of melting (Newsom and Drake 1982; Mittlefehldt and Lindstrom 2003). The opposite of this is observed in the eucrites as they contain varying W contents, with relatively constant La (Palme and Rammensee 1981; Newsom and Drake 1982; Mittlefehldt and Lindstrom 2003). On the other hand, fractional crystallization models cannot reproduce all the geochemical groups found within the eucrites (Ruzicka et al. 1997; Mittlefehldt and Lindstrom 2003).

More recently, the idea of a magma ocean on Vesta has been suggested (e.g., Righter and Drake 1997; Ruzicka et al. 1997). Ruzicka et al. (1997) suggested that the diogenites formed by crystal accumulation in a magma ocean cumulate pile, with the eucrites being the result of fractional crystallization of the resulting residual melts. Although such a model can explain the majority of the HEDs, it still evokes fractional crystallization and therefore cannot produce the geochemical groups in the eucrites. Righter and Drake (1997) also envisaged a magma ocean formation model for Vesta. Their model differed from that of Ruzicka et al. (1997) as they proposed equilibrium crystallization in a convecting magma ocean. As convection starts to slow toward the end of crystallization, there is a change in regime as equilibrium crystallization can no longer occur. Residual magmas are extruded and these undergo fractional crystallization. Although this model appears able to explain the geochemical trends within the eucrites, it does not match what is seen in the diogenites because equilibrium crystallization would produce little to no variations in trace and incompatible element compositions within mineral grains (Mittlefehldt and Lindstrom 2003), and the orthopyroxene in diogenites shows large variations (Mittlefehldt 1994). In general, it appears that no single model proposed thus far is capable of producing the geochemical diversity present among the basaltic eucrites through a single crystallization process (Mittlefehldt and Lindstrom 2003).

Eucrite Mineral Spectra

The eucrites are basalts and gabbros comprised primarily of plagioclase and pyroxenes. Pyroxene dominates the visible–near infrared (VNIR) spectra of

eucrites (Gaffey 1976), with distinctive absorption features near 1 and 2 μm (Adams 1974, 1975; Burns 1993). The positions of the absorption bands are directly proportional to the cations in the octahedral sites, primarily Ca^{2+}, Mg^{2+}, and Fe^{2+}, although other less abundant cations such as Ti^{4+}, Cr^{3+}, and Al^{3+} may also have an effect (Adams 1974; Burns 1993). Both 1 and 2 μm bands shift to longer wavelengths with an increase in calcium content (Adams 1974, 1975; Cloutis and Gaffey 1991; Burns 1993). Fe^{2+} in the higher asymmetric M2 site results in a much stronger 1 μm feature and is solely responsible for the 2 μm feature (Burns 1993). In low-calcium pyroxenes (LCP) Fe^{2+} occurs principally in the M2 site. In HCP, Ca^{2+} preferentially fills the M2, and Fe^{2+} is concentrated in the M1 site (Burns 1993). In the relatively symmetric M1 site, Fe^{2+} causes a weak absorption in the 1 μm region (more symmetry leads to a weaker absorption feature) and a second feature centered at 1.2 μm (Burns 1993). Cr^{3+}, which is present in eucrite pyroxenes, results in an absorption feature around 0.6 μm when it is located in the M1 site (Rossman 1980; Burns 1993; Cloutis 2002).

Plagioclases with Fe^{2+} incorporated into their crystal structure exhibit a weak absorption feature that lies between 1.1 and 1.3 μm (Adams and Goullaud 1978). This absorption feature has been used to infer the presence of plagioclase in spectra from Vesta (McCord et al. 1970; McFadden and McCord 1978; Adams et al. 1979), along with other basaltic asteroids (Hardersen et al. 2004). Not all plagioclases contain iron and this feature is absent in their spectra. Pieters et al. (2005) measured VNIR spectra of plagioclase mineral separates from cumulate eucrite Yamato-980318 and observed no absorption feature at 1.2 μm. However, as discussed above, this spectral region is also the location of a weak M1 pyroxene absorption band (Burns 1993; Sunshine and Pieters 1993; Klima et al. 2008), causing ambiguity in the interpretation of the spectra at approximately 1.2 μm. Many of the unbrecciated eucrite spectra show an absorption band at around 1.2 μm. This feature is stronger and, therefore, more visually obvious in the basaltic eucrites than in the cumulates (Fig. 1) (Klima et al. 2008). Here, we examine the spectra of pyroxene-plagioclase mixtures to help elucidate the spectral effect of plagioclase in the presence of pyroxene, as in the case of the eucrites.

The opaque minerals (primarily ilmenite and chromite, with lesser amounts of native iron-nickel metal and troilite) may also influence the reflectance spectra of eucrites. Their presence is often associated with the low albedos of some meteorites (Johnson and Fanale 1973), as opaques are often dark and spectrally

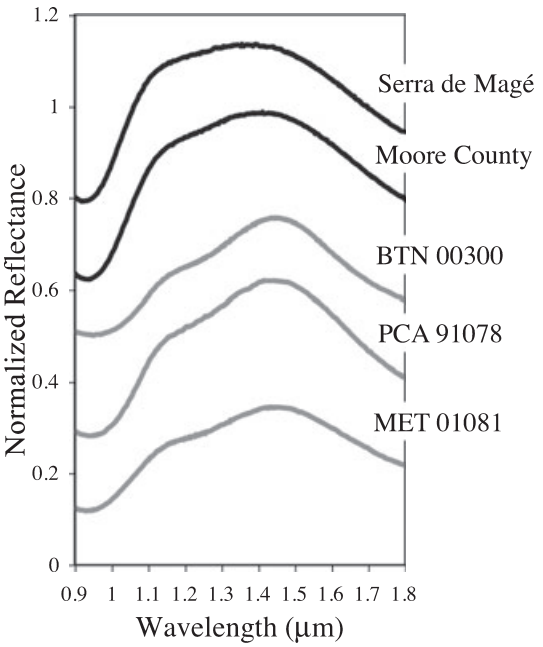

Fig. 1. Portion of VNIR spectra for unbrecciated eucrites showing the 1.2 μm absorption. The basaltic eucrite spectra are given in dark gray and the cumulate eucrites in black. The 1.2 μm absorption feature is more visually obvious in the basaltic eucrite spectra. This is a function not of plagioclase but rather the higher modal abundance of HCP in the basaltic eucrites relative to the cumulate eucrites.

featureless (Cloutis et al. 1990) and can suppress the absorption bands from the major Fe^{2+} silicates (Miyamoto et al. 1982). This effect will vary depending on the composition of the opaque minerals present, their overall modal abundance, and grain size.

METHODOLOGY

Sample Selection

For this study, each of the 29 unbrecciated eucrites studied by Mayne et al. (2009) was examined to determine the degree of terrestrial alteration. The presence of weathering products typically causes a change in spectral slope (e.g., Salisbury and Hunt 1974; Gooding 1981). Samples containing terrestrial alteration were not used for spectral work. The remaining unweathered, unbrecciated eucrites were then narrowed to 10 samples which best represented the unbrecciated eucrite suite (Table 1). Graves Nunataks (GRA) 98098, although somewhat weathered, was chosen as the 11th sample for spectral analysis because it is texturally unique, containing unusually large, elongate silica grains that overgrow or enclose the grains around them (Mittlefehldt and Lee 2001; Mayne et al. 2009).

Table 1. Modal mineralogy for the unbrecciated eucrites and LCP/HCP ratios calculated for the eucrites and mixtures.

	Modal mineralogy measured from thin section						Modal mineralogy calculated from MGM[a]		
	Plag	Pyx	LCP	HCP	Si	OSM	Actual HCP	HCP MGM 1 μm	HCP MGM 2 μm
ALHA81001	61.0	39.0	28.0	11.0	0.0	0.0	28	N/A	N/A
BTN 00300	48.4	45.7	18.7	27.0	4.8	1.0	59	73	71
Chervony Kut	45.0	51.5	22.5	29.0	1.9	1.5	56	61	61
EET 87520	48.5	49.8	28.6	21.2	1.4	0.2	43	65	63
GRA 98098	41.0	50.2	25.9	24.3	8.2	0.6	48	55	59
Ibitira	41.4	53.3	28.6	24.7	4.4	0.9	46	56	44
MAC 02522	41.1	56.6			1.6	0.7	N/A	N/A	N/A
MET 01081	40.3	53.0	25.6	27.4	5.5	1.2	52	55	57
Moore County	43.8	52.2	29.6	22.5	3.4	0.7	43	47	35
PCA 91078	45.7	50.7	25.4	25.3	2.9	0.8	50	63	67
Serra de Magé	52.7	45.1	39.7	5.4	0.7	1.5	12	18	25
Mixture 1							50	50	45
Mixture 2							15	10	19

Note: OSM = Oxides, sulfides, and metal; Si = SiO_2; Plag = plagioclase; Pyx = total pyroxene (LCP + HCP, if present); LCP = low-Ca pyroxene; HCP = high-Ca pyroxene; MGM = modified Gaussian model.
[a]Where % HCP and LCP have been normalized to 100%.

Pyroxene Characterization

Chemical analyses of pyroxene were made using the Cameca SX-50 electron microprobe (EMP) at the University of Tennessee, Knoxville. Analytical conditions were: 15 kV, 30 nA, and 1 μm beam size.

Low-resolution mineral maps of all 29 unbrecciated eucrites studied by Mayne et al. (2009) and high-resolution elemental X-ray maps of the eucrites studied here were collected using the JOEL JSM-840 scanning electron microscope (SEM) in the Department of Mineral Sciences at the Smithsonian Institution. Elemental X-ray maps of Ca, Si, and Al were combined to distinguish LCP and HCP and the relative proportions of each were calculated. This is important as the LCP:HCP ratio is one of the key features that can be estimated from spectra (Sunshine and Pieters 1993).

Visible and Near-Infrared Data and Modeling

Chips from eight of the 11 unbrecciated eucrites were ground to a <45 μm dry powder and VNIR (0.32–2.55 μm) spectra were collected using the bidirectional reflectance spectrometer at the NASA/Keck Reflectance Experiment Laboratory (RELAB) at Brown University (Fig. 2) (Pieters 1983; Pieters and Hiroi 2004). All samples were measured with an incidence angle of 30° and an emission angle of 0° at a sampling interval of 5 nm. Raw data were ratioed with a spectrum of calibrated halon reference standard to produce reflectance values. Spectra for Moore County, Ibitira, and Serra de Magé were already available from the RELAB database (Hiroi et al. 2001). These spectra were measured from <25 μm powders over the wavelength range 0.3–2.6 μm. All raw data were ratioed with a calibrated halon reference standard spectrum to produce reflectance values.

Band centers were measured using the method of Gaffey et al. (1993). The resulting band centers are referred to as "continuum-removed band centers" throughout the rest of this study. The collected spectra were also analyzed using the modified Gaussian model (MGM) (Sunshine et al. 1990; Sunshine and Pieters 1993). The MGM models each spectrum as a continuum and a series of modified Gaussian distributions, with each distribution curve representing a specific absorption band characterized by three parameters: band strength, band center, and band width (Sunshine et al. 1990). This approach successfully resolves the absorptions of overlapping bands (Mustard 1992; Sunshine and Pieters 1993; Sunshine et al. 1993; Schade and Wäsch 1999; Kanner et al. 2007; Klima et al. 2007). MGM offers a useful approach for modeling the spectra of the eucrites, which are dominated by overlapping absorptions due to the presence of both LCP and HCP bands in both the 1 and 2 μm regions. Each spectrum was initially modeled using just one pyroxene, whose composition was allowed to vary. The MGM outputs a wavelength-dependent RMS error and this shows characteristic features (peak errors offset from band centers) that are diagnostic of missing bands (Sunshine and Pieters 1993). If these errors were observed then the spectrum was modeled using a two-pyroxene model, consisting of one low-Ca pyroxene and one high-Ca pyroxene. Additional bands were only added if the RMS error indicated that

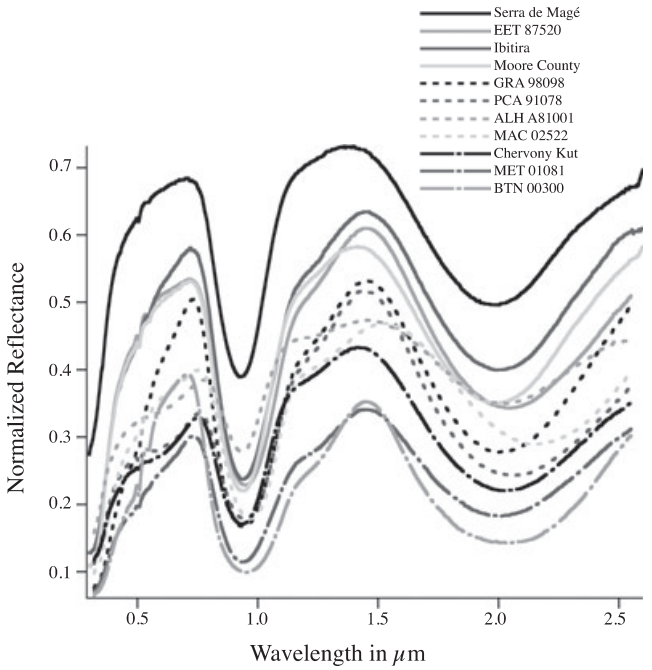

Fig. 2. VNIR spectra collected of the unbrecciated eucrites. Variations in band centers, absorption depths, and spectral contrast can be seen between the spectra.

they were required. All band centers derived from the MGM are referred to here as "MGM-derived band centers."

As part of a broader study of spectral mixtures (McCoy et al. 2007; Corrigan et al. 2007), two sets of powder mixtures were produced containing LCP, HCP, and plagioclase, with one set having an LCP:HCP ratio of 50:50, and the other 85:15. For each of the two sets, a sequence of mixtures was prepared with different proportions of plagioclase, ranging from 10% to 50% for 85:15 and from 10% to 60% for 50:50, increasing in increments of 10%. The standards used within the mixtures were Johnstown hypersthene from the Johnstown meteorite, the terrestrial Kakanui augite, and Lake County plagioclase (Table 2a) (Jarosewich et al. 1979). These samples were chosen as they are part of the Smithsonian Microprobe Standard Reference Collection and have been chemically well characterized and are in common use as mineralogical standards. The eucrites are predominantly LCP, HCP, and plagioclase mixtures and, therefore, the mixtures lend themselves well to comparisons with eucrite spectra.

All the standards were ground and sieved to <45 μm powders. Spectra were collected of both the mixtures and the individual standards that compose them using the same method as described for the eucrites. Continuum-removed band centers and MGM-derived band centers were calculated as described above.

Table 2a. Compositional data for endmembers used in the pyroxene-plagioclase mixtures.

	Johnstown hypersthene	Kakanui augite	Lake Co. plagioclase
SiO_2	54.09	50.73	51.25
Al_2O_3	1.23	8.73	30.91
Fe_2O_3		1.08	0.34
FeO	15.22	5.37	0.15
MgO	26.79	16.65	0.14
CaO	1.52	15.82	13.64
Na_2O	<0.05	1.27	3.45
K_2O	<0.05	0.00	0.18
TiO_2	0.16	0.74	0.05
P_2O_5			
MnO	0.49	0.13	0.01
Cr_2O_3	0.75		
H_2O	0.00	0.04	0.05
Total	100.25	100.56	100.17
Wo	3.00	36.01	
En	73.56	52.72	
Fs	23.44	11.27	
An			80.86
Ab			18.51
Or			0.64

Note: The compositional data given here are from Jarosewich et al. (1979).

Table 2b. MGM results for Johnstown hypersthene and Kaknui augite.

	Johnstown	Kaknui
MGM band centers (μm)		
Additional M1	0.85	0.77
1 μm band	0.94	1.00
1.2 feature	1.14	1.21
2 μm band	1.88	2.26
MGM band strengths (log reflectance)		
Additional M1	−0.48	−0.19
1 μm band	−1.16	−0.84
1.2 feature	−0.15	−0.25
2 μm band	−0.96	−0.45
MGM band widths (μm)		
Additional M1	0.16	
1 μm band	0.18	0.22
1.2 feature	0.27	0.34
2 μm band	0.64	0.64

Note: MGM = modified Gaussian model.

RESULTS

Pyroxene-Plagioclase Mixtures

Individual spectra of the pyroxene and plagioclase standards used to construct the mixtures were collected (Fig. 3a) (McCoy et al. 2007; Corrigan et al. 2007) and MGM was applied to the two pyroxene spectra (Fig 3; Table 2b). The Lake County plagioclase spectrum shows

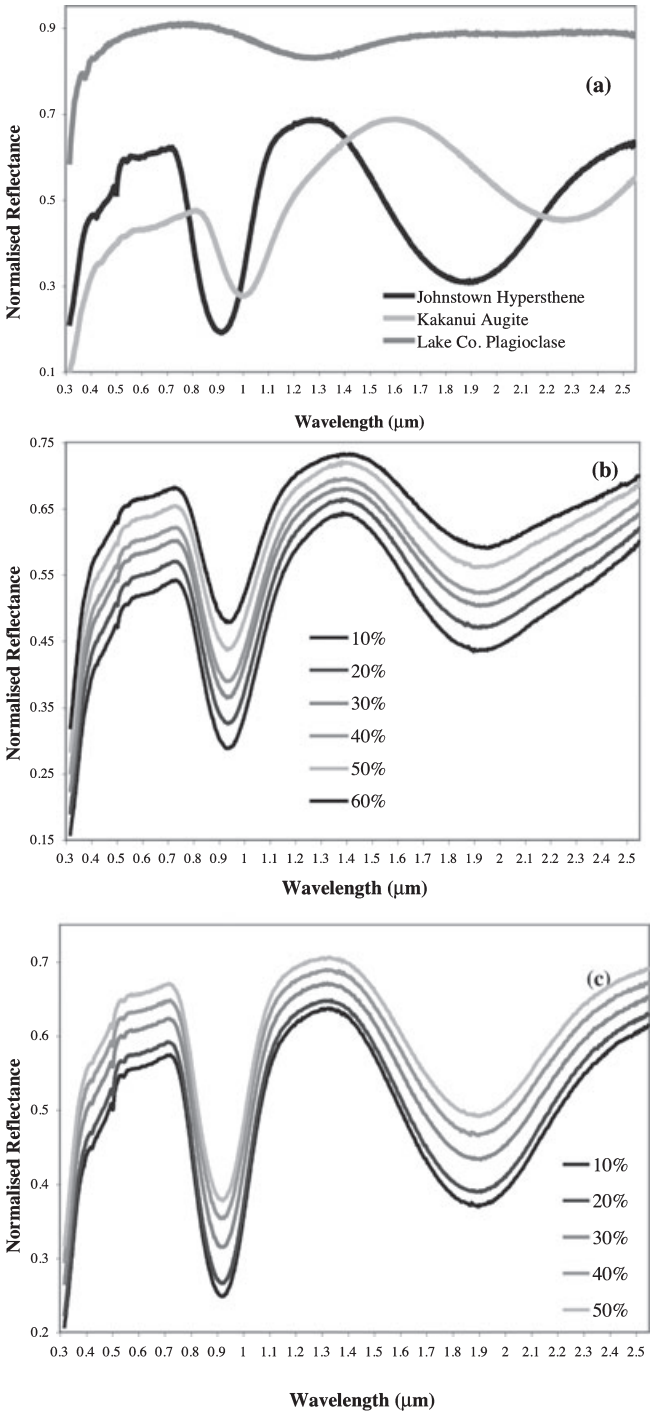

Fig. 3. Reflectance spectra of (a) mineral standards used in the mixtures, (b) 50:50 LCP:HCP mixtures with increasing plagioclase abundance, (c) 85:15 LCP:HCP mixtures with increasing plagioclase abundance. The spectrum for Lake County plagioclase has an absorption feature at 1.2 μm. However, this absorption cannot be visually distinguished in the mixture spectra. The mixtures show increased absolute reflectance with increasing plagioclase contents, but no other changes in the spectra are observed.

a broad absorption feature between 1.2 and 1.3 μm, due to Fe^{2+} in this plagioclase. This feature is not found in all plagioclases and is particularly strong in the Lake County spectrum. The spectra of Kakanui augite and Johnstown hypersthene also have a 1.2 μm absorption feature as a result of Fe^{2+} in the M1 site. This 1.2 μm feature in pyroxene is only visually apparent in Kakanui augite, but MGM confirms its presence in Johnstown (and most LCPs) (Fig. 4) (Sunshine and Pieters 1993).

As expected, Kakanui augite (HCP) has band centers at significantly longer wavelengths than Johnstown hypersthene (LCP), due to the greater Ca content in Kakanui. Both endmember pyroxene spectra required the addition of an additional weak approximately 1 μm band (0.87–0.88 μm) in the MGM fit. This band results from Fe^{2+} in the M1 octahedral site and is predicted by theory (Burns 1993), but often masked by the larger M2 band in the same wavelength region. This band is much stronger in Johnstown, reflecting its higher iron content (Fs_{23} versus Fs_{11}) (Jarosewich et al. 1979). HCP from the Martian meteorite Nakhla also required the additional 1 μm M1 band (at 0.92 μm) to achieve a good fit (Sunshine et al. 2004a). Nakhla pyroxenes are also FeO-rich with predominantly augite cores of iron composition approximately Fs_{26}, increasing to Fs_{44} at the rim (e.g., Treiman 1990; Harvey and McSween 1992; McSween and Treiman 1998).

The pyroxene–plagioclase mixture spectra were all fit with the same two-pyroxene model. The starting parameters for this model are given in Table 4a. All the mixture spectra are dominated by the two pyroxenes and to the naked eye there is no discernable feature around 1.2 μm (Figs. 3b and 3c). Neither set of mixture spectra shows a significant shift in continuum-removed band centers with the addition of extra plagioclase (Table 3). Overall reflectance increases with increasing plagioclase abundance, and the 85:15 mixtures have higher reflectance than the 50:50. The mixtures were all modeled using MGM (Fig. 5). Each spectrum required two pyroxenes and the addition of the weak approximately 1 μm M1 band (0.87–0.88 μm) that results from Fe^{2+} in the M1 octahedral site. The need for the extra 1 μm M1 band is not unexpected as both the endmember pyroxenes required it in their individual models. LCP:HCP ratios (the ratio of the relative strength of the LCP band to the relative strength of the HCP band) calculated using MGM can be used to predict the relative abundance of HCP in each sample (Table 1) (Sunshine et al. 1993). The predicted values of HCP in the mixtures were within ±5% of the actual values (Table 1).

Despite the addition of up to 60% plagioclase in the mixtures none of the spectra required an additional

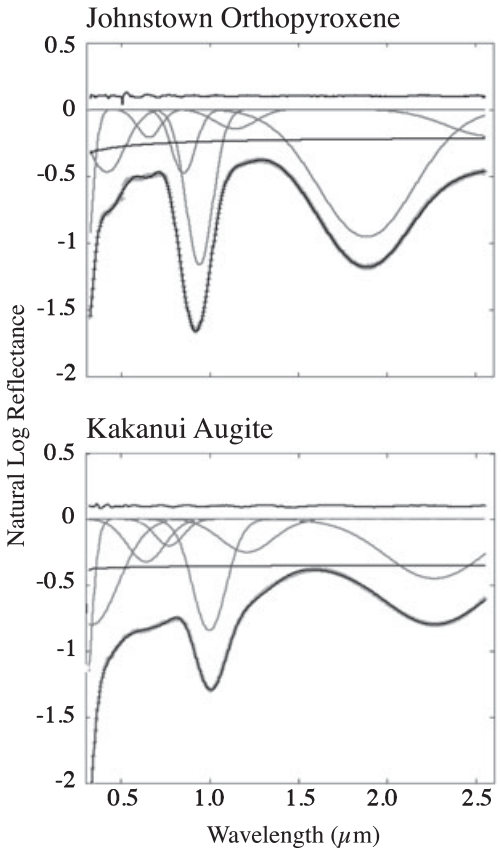

Fig. 4. MGM results for endmember pyroxenes, Johnstown hypersthene, and Kakanui augite. The individual absorption bands modeled by modified Gaussians are shown in dark gray. The upper black line represents the residual error of the model; the lower black line represents the continuum. The measured spectrum is plotted with gray +s, and the black is the modeled value. The Kakanui augite can be seen to have a deeper 1.2 μm band absorption than the Johnstown hypersthene. The 1.2 μm feature is often more prominent in HCP-like Kakanui augite as there is more Fe^{2+} in the M1 site (the cause of the absorption) due to Ca^{2+} preferentially filling the M2 site.

band in the 1.2 μm region to account for the presence of plagioclase. Band widths remain constant with increasing plagioclase abundance, as do the MGM-derived band centers for the separate LCP and HCP bands and the relative strengths of the two bands (LCP/HCP at 1 and 2 μm) (Table 3). To examine changes in the 1.2 μm region that may be attributed to plagioclase, we calculated the strength of the 1.2 μm band relative to the combined strengths of the 1.2 and 2 μm HCP band (Fig. 6). This should minimize the effects of pyroxene in this region as with increasing plagioclase you might expect the 1.2 μm feature to strengthen and the 2 μm HCP band to remain constant. Yet, very minimal change in the calculated ratio was observed (Fig. 6). GRA 98098 and Serra de Magé have similar LCP:HCP ratios to the mixture sets, 52:48 and 88:12, respectively. When you compare their plagioclase content and ratio—Strength (1.2/[1.2 + 2 μm HCP])—to those of the mixtures it can be seen that they do not fall on the line that corresponds to their LCP/HCP ratios (Fig. 6).

The results here strongly indicate that the 1.2 μm absorption is not a result of the plagioclase content of the sample. Instead, as discussed above, it is due to Fe^{2+} in the M1 site of pyroxene, resulting in a weak absorption in the 1 μm region and a second feature centered at 1.2 μm (Burns 1993).

Eucrite Pyroxene Chemistry and Modal Mineralogy

The pyroxenes in the 11 eucrites are plotted with respect to their quadrilateral compositions and their minor elements (Fig. 7). A full discussion of pyroxene compositional differences within the unbrecciated eucrites can be found in Mayne et al. (2009).

The modal mineralogy for all 11 unbrecciated eucrites calculated from a combination of previously reported SEM mineral maps and the high-resolution pyroxene mapping is given in Table 1. The LCP:HCP ratios for Chervony Kut, Moore County, and Serra de Magé were found to be in close agreement with those collected by Delaney and Prinz (1984) using EMP analyses.

Examples of mapped tiles that show the range of exsolution textures within eucrite pyroxenes are given in Fig. 8. The percentage of HCP varies from grain to grain (Fig. 8a) with HCP as both exsolution within LCP and as individual grains (Fig. 8b). Different exsolution morphologies are also present within and between individual meteorites as some contain HCP blebs and others more elongate lamellae (Fig. 8c). The modal abundance of pyroxene (LCP + HCP) ranges from 39.0% to 56.6%. Total HCP varies from 5.4% to 29.0% (Table 1) and does not covary with the total modal percentage of pyroxene. Overall, the cumulate eucrite Serra de Magé has the lowest percentage of HCP and this percentage did not vary greatly from grain to grain within the thin section. Allan Hills (ALH) A81001 is the only unbrecciated eucrite studied that contains phenocrysts. The phenocrysts have an LCP composition (Wo_{1-2}) while the pyroxene in the rest of the sample has a higher Ca content ($Wo_{>20}$) (Mayne et al. 2009). This meteorite has the second lowest modal percentage of HCP (11%).

Modeling of the Unbrecciated Eucrites

As with the mixtures, initial modeling of all 11 eucrite spectra revealed that none required an additional band for plagioclase (Fig. 9). Six of the unbrecciated

Table 3. MGM results for plagioclase–pyroxene mixtures.

	50–50 (LCP–HCP)							85–15 (LCP–HCP)					
% Plagioclase	0	10	20	30	40	50	60	0	10	20	30	40	50
Continuum-removed band centers (μm)													
Band 1	0.94	0.94	0.94	0.94	0.94	0.94	0.94	0.92	0.92	0.92	0.92	0.92	0.92
Band 2	1.92	1.92	1.92	1.93	1.93	1.92	1.93	1.89	1.89	1.89	1.89	1.89	1.89
MGM band centers (μm)													
Additional M1	0.87	0.87	0.87	0.87	0.87	0.87	0.88	0.88	0.88	0.88	0.88	0.88	0.88
LCP at 1	0.92	0.92	0.92	0.92	0.92	0.92	0.92	0.92	0.93	0.93	0.92	0.92	0.92
HCP at 1	1.02	1.01	1.02	1.02	1.01	1.01	1.01	1.01	1.01	1.01	1.01	1.01	1.01
1.2 feature	1.16	1.17	1.17	1.17	1.17	1.18	1.18	1.14	1.14	1.14	1.14	1.14	1.14
LCP at 2	1.88	1.88	1.88	1.88	1.88	1.88	1.89	1.87	1.87	1.87	1.87	1.87	1.87
HCP at 2	2.32	2.32	2.33	2.32	2.31	2.30	2.30	2.23	2.23	2.23	2.23	2.23	2.23
MGM band strengths (log reflectance)													
Additional M1	−0.20	−0.19	−0.16	−0.13	−0.13	−0.10	−0.08	−0.14	−0.20	−0.18	−0.10	−0.08	−0.05
LCP at 1	−0.55	−0.52	−0.47	−0.43	−0.39	−0.33	−0.28	−0.85	−0.80	−0.76	−0.69	−0.62	−0.60
HCP at 1	−0.27	−0.30	−0.26	−0.22	−0.21	−0.19	−0.17	−0.04	−0.04	−0.04	−0.04	−0.03	−0.03
1.2 feature	−0.13	−0.13	−0.11	−0.10	−0.09	−0.09	−0.07	−0.10	−0.10	−0.09	−0.08	−0.07	−0.06
LCP at 2	−0.43	−0.41	−0.37	−0.32	−0.30	−0.26	−0.23	−0.58	−0.58	−0.55	−0.47	−0.42	−0.39
HCP at 2	−0.20	−0.20	−0.18	−0.15	−0.14	−0.13	−0.10	−0.10	−0.10	−0.09	−0.08	−0.07	−0.06
LCP/HCP at 1	2.03	1.74	1.83	1.91	1.83	1.72	1.71	19.41	18.91	21.60	16.94	18.12	21.47
LCP/HCP at 2	2.20	2.06	1.99	2.07	2.15	2.10	2.32	5.76	5.76	6.37	6.17	6.35	6.94
MGM band widths (μm)													
Additional M1	0.19	0.19	0.19	0.19	0.19	0.19	0.19	0.19	0.19	0.19	0.19	0.19	0.19
LCP at 1	0.19	0.19	0.19	0.19	0.19	0.19	0.19	0.19	0.19	0.19	0.19	0.19	0.19
HCP at 1	0.20	0.20	0.20	0.20	0.20	0.20	0.20	0.20	0.20	0.20	0.20	0.20	0.20
1.2 feature	0.28	0.28	0.28	0.28	0.28	0.28	0.28	0.28	0.28	0.28	0.28	0.28	0.28
LCP at 2	0.54	0.54	0.54	0.54	0.54	0.54	0.54	0.56	0.56	0.56	0.55	0.55	0.55
HCP at 2	0.57	0.57	0.57	0.57	0.57	0.57	0.57	0.57	0.57	0.57	0.57	0.57	0.57

Note: MGM = modified Gaussian model; LCP = low-Ca pyroxene; HCP = high-Ca pyroxene.

Table 4a. Model parameters of absorption bands in the MGM fits for the pyroxene–plagioclase mixtures.

Continuum offset	0.47			
Continuum slope	−1.25E-06			
	Absorption	Band center (μm)	Band width (μm)	Band strength
Band 1	Charge transfer	0.284	0.095	−1.046
Band 2	Charge transfer	0.403	0.328	−0.48
Band 3	Cr^{3+}	0.662	0.145	−0.102
Band 4	Additional M1	0.878	0.188	−0.156
Band 5	LCP 1 μm	0.908	0.188	−0.156
Band 6	HCP 1 μm	1.014	0.193	−0.551
Band 7	1.2 μm	1.148	0.278	−0.068
Band 8	LCP 2 μm	1.832	0.56	−0.137
Band 9	HCP 2 μm	2.266	0.563	−0.449
Band 10	Adsorbed water band	2.666	0.563	−0.449

Note: MGM = modified Gaussian model; LCP = low-Ca pyroxene; HCP = high-Ca pyroxene.

eucrites were well-fit using a two-pyroxene, nine-band model (Table 4b). Both Bates Nunataks (BTN) 00300 and Chervony Kut required the addition of the weak Fe^{2+} M1 band in the 1 μm region (at 0.83 and 0.87 μm, respectively) for a good fit, as with the pyroxene mixtures. These two samples have the lowest LCP:HCP ratio (Table 1) and it is most likely that it is the high-Ca content of the pyroxenes, which results in the M1 1 μm band being required in the model for these samples. Ca^{2+} preferentially fills the M2 site, pushing Fe^{2+} into the M1 (Burns 1993), resulting in a stronger M1 band in the 1 μm region. Increased Ca-composition within pyroxene also pushes the band 1 and band 2 centers to longer wavelengths (Adams 1974, 1975; Cloutis and Gaffey 1991), which may act to further distinguish the M1 band. MGM-derived band centers and relative strengths for the unbrecciated eucrites are given in Table 5. The separate MGM-derived LCP and HCP band centers are compared to the continuum-removed band centers for pyroxenes in Fig. 10.

MacAlpine Hills (MAC) 02522 is the only eucrite here that contains zoned pyroxene. This meteorite was well-fit by one HCP, with a broad band in the 2 μm region (0.7 μm compared to <0.6 μm for all other samples) (Table 5). Anomalously wide bands are a characteristic of continuous zoning and rapid cooling (Sunshine and Pieters 1993). The additional Fe^{2+} M1 1 μm band was again needed (at 0.88 μm) due to the

Table 4b. Bands required in MGM for each of the unbrecciated eucrite spectra.

	Absorption	ALHA 81001	BTN 00300	Chervony Kut	EET 87520	GRA 98098	Ibitira	MAC 02522	MET 01081	Moore County	PCA 91078	Serra de Magé
Band 1	Charge transfer	Y	Y	Y	Y	Y	Y	Y	Y	Y	Y	Y
Band 2	Charge transfer	Y	Y	Y	Y	Y	Y	Y	Y	Y	Y	Y
Band 3	Cr^{3+}	Y	Y	Y	Y	Y	Y	Y	Y	Y	Y	Y
Band 4	Additional M1	N	Y	Y	N	N	N	Y	N	N	N	N
Band 5	LCP 1 μm	N/A*	Y	Y	Y	Y	Y	N/A*	Y	Y	Y	Y
Band 6	HCP 1 μm	N/A*	Y	Y	Y	Y	Y	N/A*	Y	Y	Y	Y
Band 7	1.2 μm	Y	Y	Y	Y	Y	Y	Y	Y	Y	Y	Y
Band 8	LCP 2 μm	N/A*	Y	Y	Y	Y	Y	N/A*	Y	Y	Y	Y
Band 9	HCP 2 μm	N/A*	Y	Y	Y	Y	Y	N/A*	Y	Y	Y	Y
Band 10	Adsorbed water band	Y	Y	Y	Y	Y	Y	Y	Y	Y	Y	Y

Note: MGM = modified Gaussian model; LCP = low-Ca pyroxene; HCP = high-Ca pyroxene.
N/A* for band numbers 5, 6 and 8, 9 denotes eucrites that only needed one pyroxene in the model and, therefore, did not have separate LCP and HCP bands in these regions.
All the unbrecciated eucrite spectra require bands at 0.6 μm (Cr^{3+}) and 1.2 μm for good MGM fits. However, these two features are not observable in the overall spectrum of all of the eucrites (see the Primitive Versus Evolved Magmas section for more details on the 0.6 μm feature).

high iron content of the pyroxenes in MAC 02522 ($\sim Fs_{55}$). The ALHA81001 spectrum was modeled well using a seven-band, one-pyroxene model (Fig. 9), although it actually contains two pyroxenes. ALHA81001 is the finest grained eucrite studied here and although it contains petrologically distinct LCP and HCP it appears that the spectral model yields one pyroxene with a composition representing an average of the two.

Chervony Kut, GRA 98098, Moore County, and Serra de Magé all show a nonrandom residual error in the 1 μm region of the MGM model. The peak error occurs at the same point as the MGM-derived band center. This may indicate band saturation, as errors arising from missing absorption bands tend to be offset and much larger (Sunshine and Pieters 1993). However, we are only examining major absorption features here and it is possible that the addition of extra bands, such as those that represent spin-forbidden pyroxene features, may also improve upon this error (Burns 1993; Klima et al. 2007).

The MGM-derived LCP band center for BTN 00300 in the 2 μm region is at much shorter wavelengths than the other eucrites. There are no compositional differences between BTN 00300 and the other eucrites that would explain the difference in the MGM-derived band centers. BTN 00300 spectrum has the deepest, strongest bands of all the eucrites. BTN 00300 also contains the highest HCP content and is relatively rich in opaque minerals. In this case, spectral modeling is not consistent with the observed petrology. It is possible that we are not seeing enough of the 2 μm band to achieve a good MGM fit. Site occupancies within the pyroxenes can also affect their spectra. Mössbauer spectroscopy was performed on BTN 00300 along with Elephant Moraine (EET) 87520 and MAC 02522, which had simpler spectra to model. All three Mössbauer spectra are dominated by Fe^{2+} in pyroxene and show approximately the same M1:M2 area ratio suggesting that they have very similar site occupancies. This indicates that the differences in the BTN 00300 spectra are not due to site occupancy and instead are more likely related to its differing modal mineralogy.

WHAT CAN WE LEARN ABOUT PETROLOGY FROM SPECTRA?

Asteroidal differentiation and crust formation can be conceptually understood as the crystallization of basaltic to ultramafic melts with the composition of the melt and the extent of crystallization determining the minerals formed, their abundances and compositions. Cooling and metamorphism of the crust have the potential to further alter the minerals present and their compositions through diffusion, including exsolution. In this section, we examine whether we can accurately model the spectra of petrologically characterized eucrites studied by Mayne et al. (2009) to predict their mineralogy, mineral abundances, and mineral compositions.

Modal Mineralogy

Low-Calcium to High-Calcium Pyroxene Ratio

High-calcium pyroxene can be used as a tracer of igneous history as it is one of the key spectrally observable minerals formed during differentiation of a chondritic asteroid (Sunshine et al. 2004b). We know

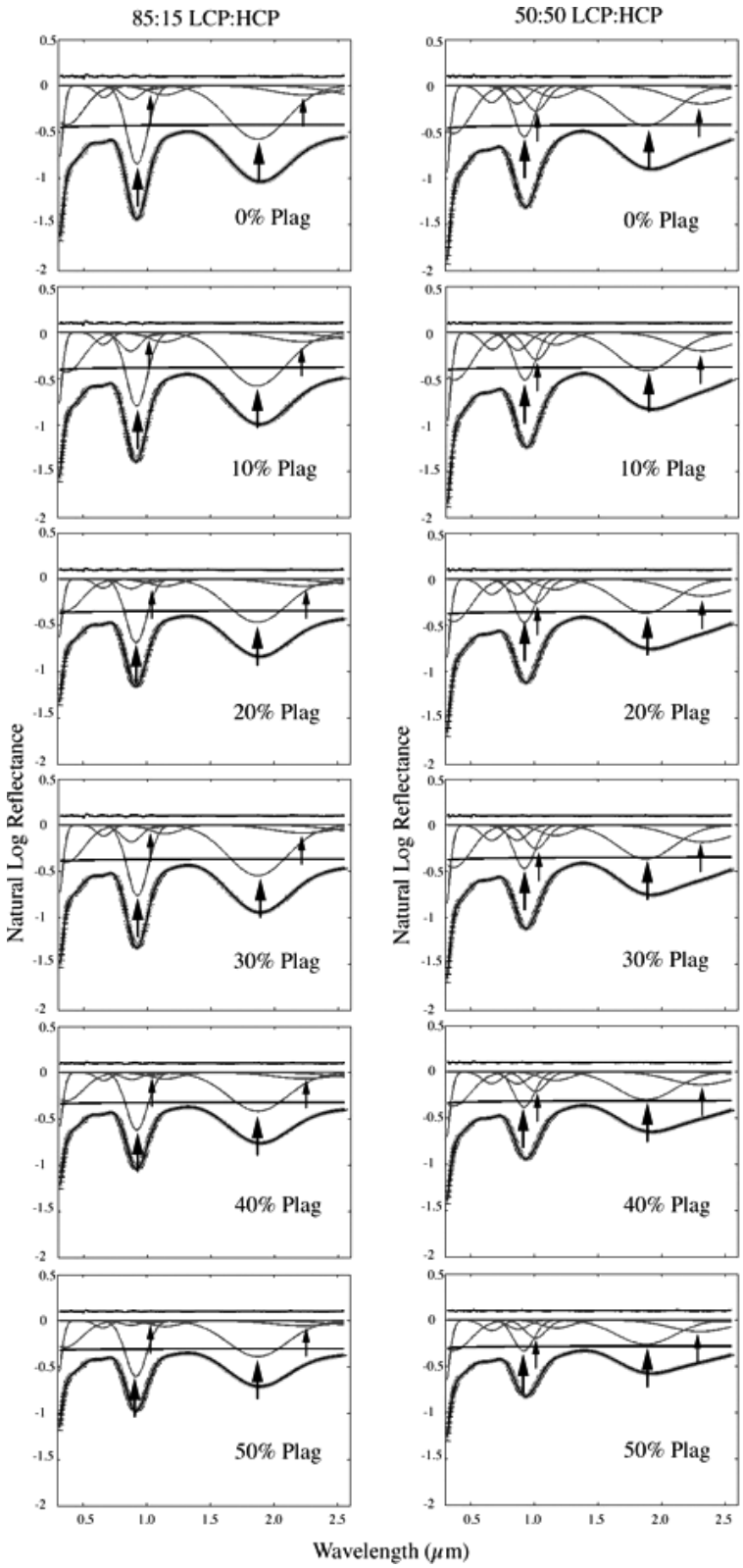

Fig. 5. MGM results for all mixture spectra. The individual absorption bands modeled by modified Gaussian curves are shown in dark gray. Lines and symbols as given in Fig. 4. A large arrow is used to denote the LCP band in the 1 and 2 μm region, and a small arrow for HCP. The HCP bands are stronger in the 50:50 mixture set because they have a higher abundance of HCP. The strength of the 1.2 μm band does not appear to visually increase with increasing plagioclase content.

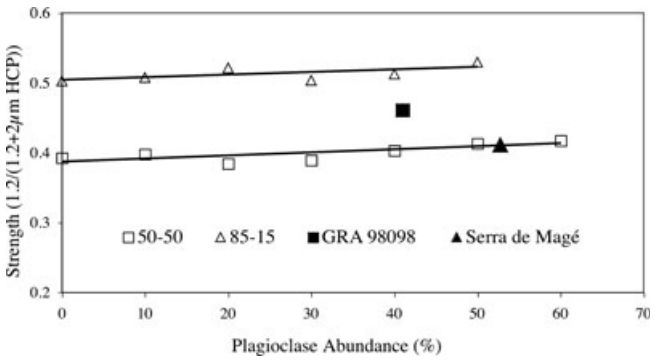

Fig. 6. The relative strength of the 1.2 μm band against plagioclase abundance for the pyroxene–plagioclase mixtures. The strength of 1.2 μm band is normalized to the strength of the 2 μm HCP band (1.2/[1.2 + 2 HCP]). If the presence of plagioclase were contributing to the 1.2 μm absorption feature, then we would expect this ratio to increase markedly with increasing plagioclase content, which is not observed. GRA 98098 and Serra de Magé, eucrites of a known composition, have LCP:HCP ratios similar to those of the mixtures: 52:48 (GRA 98098) and 88:12 (Serra de Magé). If the amount of plagioclase was affecting the ratio used in this figure then GRA 98098 and Serra de Magé should plot on the lines dictated by the mixtures and they do not. For example, Serra de Magé plots with the 50:50 mixtures, despite having a composition similar to the 85:15.

that the eucrites formed as a result of differentiation of their parent body and, as such, they contain relatively abundant HCP (5.4–29%). MGM has been used in the past as a tool for modeling the relative proportions of LCP and HCP from spectra. Sunshine et al. (1993) used MGM to model the spectra of the dual lithologies within Martian meteorite EETA79001 and found that they were able to predict the relative modal abundance of LCP and HCP within ±5–10% of those obtained from petrographic methods. More recently, Kanner et al. (2007) used MGM to model laboratory data for Martian pyroxenes and were also able to estimate the relative modal abundance of LCP and HCP within ±10%.

The eucrites represent more complex mixtures of LCP-HCP-plagioclase-opaque minerals. Calculated relative HCP abundances (i.e., where modal abundance of HCP and LCP have been normalized to 100%) from MGM (Table 1) are typically higher than those measured petrologically. The predicted relative modal abundances for HCP have a 1σ value of ±9% for the 2 μm band and ±6% for the 1 μm region (Table 1). The original calibration study by Sunshine and Pieters (1993) did not use pyroxenes with iron compositions equivalent to the eucrites, which probably accounts for the larger error in predicting the relative amounts of LCP and HCP. The fact that the relative abundances of HCP and LCP in the mixtures, which contain Fe-poor pyroxenes relative to the eucrites, were estimated to within ±5% supports this conclusion.

Basaltic versus Cumulate Eucrites

The simplest classification of the eucrites subdivides them according to their petrology into basaltic and cumulate eucrites. The cumulate eucrites tend to be coarser grained and contain pyroxenes that are Fe-poor relative to the basaltic eucrites, as well as less HCP overall. The cumulate eucrites have continuum-removed band centers at shorter wavelengths than their basaltic counterparts (Fig. 10), which are most likely a result of their lower modal HCP component. If the FeO-content of the pyroxenes were driving the continuum-removed centers to shorter wavelengths, then this same trend would be expected in the MGM-derived band centers too. The MGM-derived band centers for both LCP and HCP for basaltic and cumulate eucrites are very similar (Fig. 10), suggesting that the LCP:HCP ratio is the principal spectral variable here.

Primitive versus Evolved Magmas

The above data have shown that eucrite spectra are dominated by pyroxene. As a result, differences between eucrite spectra are driven by differences in pyroxene chemistry between samples, which in turn is influenced by the crystallization history of the eucrite studied. Major-element pyroxene chemistry (Mg, Fe, and Ca) can be used to divide the eucrites into basaltic and cumulate groups but little variation is then seen within these groupings. Mayne et al. (2009) noted that variation is present within the minor elements of pyroxene (Al, Ti, and Cr) for the basaltic eucrites. In the eucrite, basaltic melt chromium behaved as a compatible element in pyroxene, meaning that pyroxenes crystallized from a primitive melt were Cr-rich. As crystallization of pyroxene proceeded and the melt evolved, the amount of chromium in the melt decreased, driving the pyroxene to more Al-rich compositions (Pun and Papike 1996). Once plagioclase reaches the solidus it competes for the Al and pyroxenes become richer in Ti (Pun and Papike 1996).

Of the 11 unbrecciated eucrites studied here ALHA81001, Pecora Escarpment (PCA) 91078, and Chervony Kut contain pyroxene rich in Cr (Fig. 7) and, therefore, probably crystallized from a primitive magma. This interpretation is supported by ALHA81001 as it not only contains Cr-rich pyroxenes, but is also the most Mg-rich member of the Stannern trend (a geochemical grouping used to subdivide the eucrites), and, as such, is considered to be the most primitive (Mittlefehldt, personal communication). If

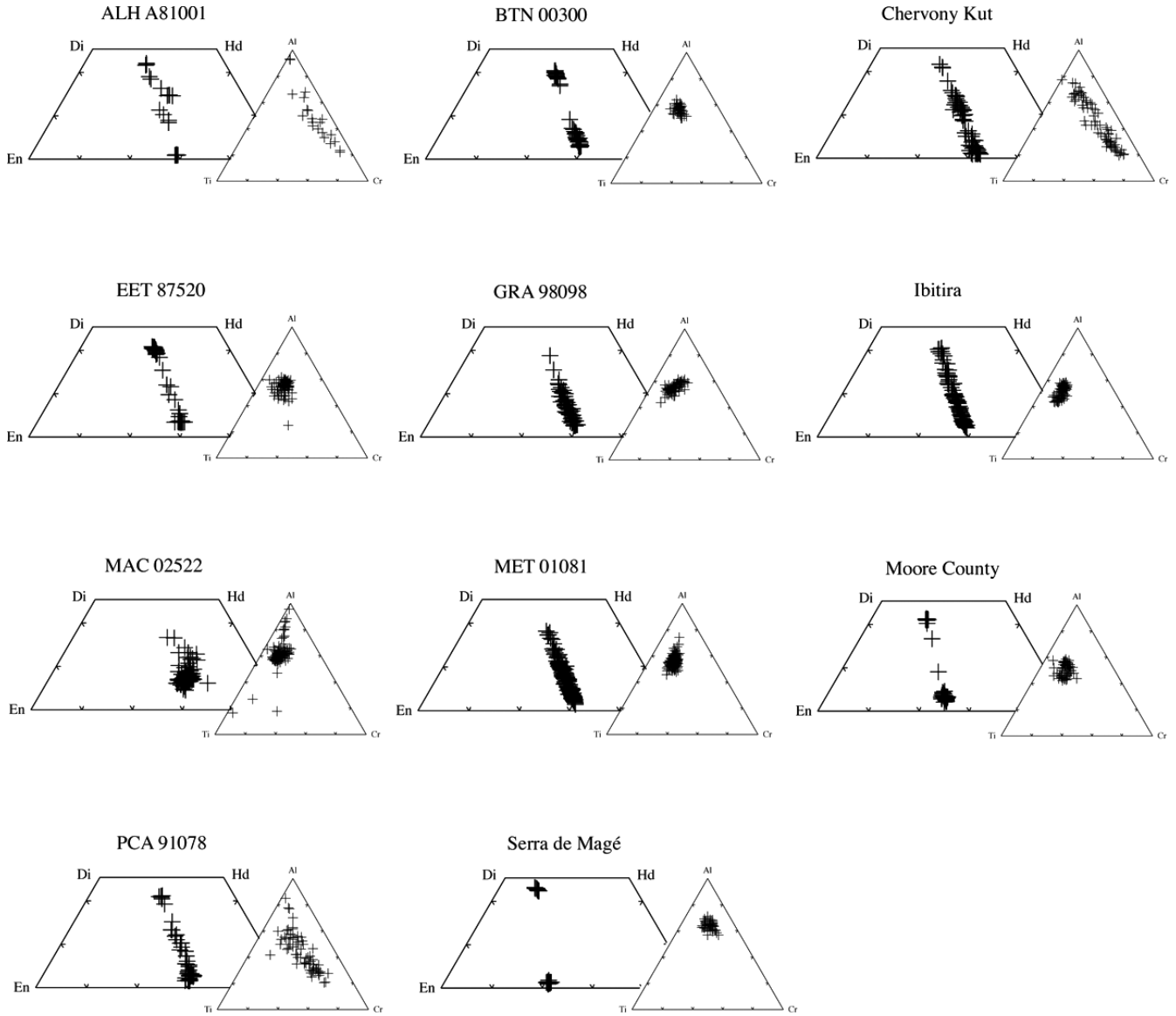

Fig. 7. Unbrecciated eucrite pyroxene compositions obtained by EMP analysis. Major-element pyroxene compositions (Fe, Mg, and Ca) are shown in the quadrilaterals and minor-element compositions (Ti, Al, and Cr) are overlain in the form of ternary plots. All ternary compositional diagrams in this article were plotted using the freeware program Δplot (John 2004). The majority of the eucrites show equilibrated quadrilateral compositions, apart from MAC 02522, which contains one zoned pyroxene. Some eucrites have not undergone metamorphic re-equilibration within the minor elements in pyroxene, e.g., Chervony Kut.

such differences in eucrite pyroxene minor element chemistry can be detected spectrally, then conclusions can be drawn regarding the magmatic evolution of the samples.

Cr^{3+} in octahedral coordination in the pyroxene M1 site is known to have absorption feature around 0.6 μm (Rossman 1980; Burns 1993; Cloutis 2002). All eucrites require this band in their MGM models irrespective of their pyroxene Cr-content (Table 4b); however, in most cases it is not a visible component of their spectra, which indicates a low Cr-content. If this feature is visible within any of the unbrecciated eucrite spectra, indicating pyroxenes with a high Cr-content, it could be used as a proxy for the relative magmatic evolution of the unbrecciated eucrites. The 0.6 μm region for the three unbrecciated eucrites that contain Cr-rich pyroxenes is shown in Fig. 11a and all three spectra show an observable feature at this wavelength that is not seen within the other eucrite spectra. Cloutis (2002) calculated that the amount of Cr^{3+} present within a pyroxene for this absorption to appear was between 0.38 and 0.9 wt% (LCP and HCP, respectively).

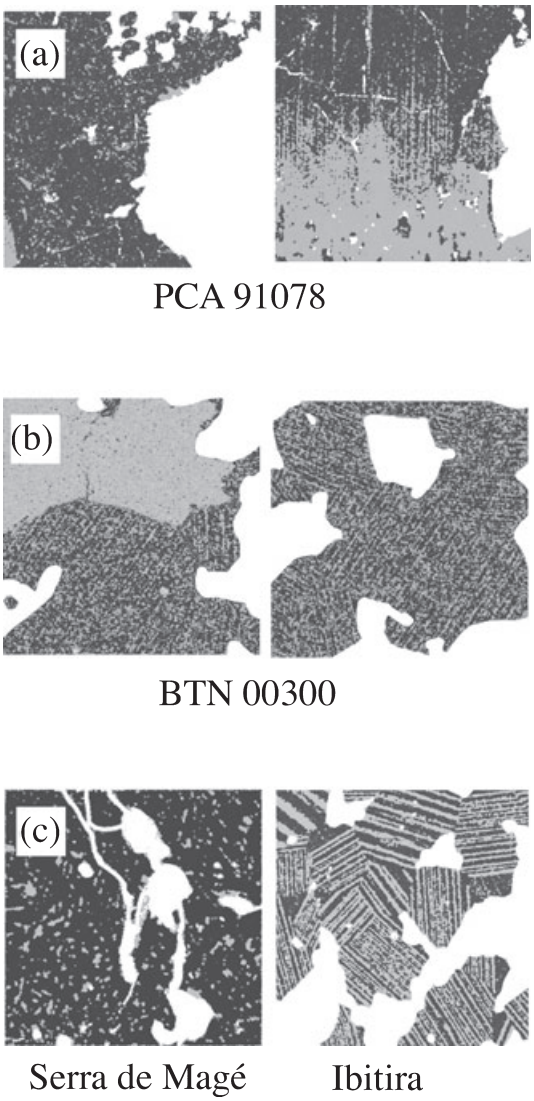

Fig. 8. High-resolution mineral maps of pyroxene compiled using SEM X-ray maps. These maps illustrate not only the differing types of exsolution morphologies within eucrite pyroxene but also the variation in scale at which they appear. LCP is shown as a dark gray and HCP as a light gray. a) Variations in the proportions of LCP and HCP within different grains. b) Individual grains of HCP and HCP exsolved from LCP. c) Different exsolution morphologies.

The three meteorites here with a visible 0.6 μm feature contain some pyroxenes with chromium compositions over 0.02 afu (atomic formula units), or approximately 0.65 wt% (Fig. 11b), which lies between the two values reported by Cloutis (2002).

Degree of Equilibration

The majority of the eucrites are metamorphosed or "equilibrated" with respect to the pyroxene quadrilateral compositions (Pun and Papike 1996). Equilibration due to metamorphism redistributes the elements throughout the pyroxene and erases the original crystallization trend, and, with it, the original zonation in the pyroxene. The minor elements within pyroxene, although less susceptible to equilibration, are also affected by it (Mayne et al. 2009). In the insets in Fig. 7, those eucrites that are equilibrated show compositions closest to the Al corner and clumped in the center between Ti and Cr. The three eucrites identified above as Cr-rich (Chervony Kut, PCA 91078, and ALHA81001) are the only samples for which the original zonation in minor-element composition can be observed (Fig. 7). This means that the presence of Cr-rich pyroxenes in a eucrite not only reveals that it crystallized from a primitive magma, but also that it is not equilibrated with respect to its minor elements and therefore underwent relatively fast-cooling without later metamorphism. Thus, the 0.6 μm feature seen in the eucrite spectra could provide a tool for interpreting the thermal history of the surface of Vesta (metamorphosed or not) as well as its evolution (Cr-rich and therefore primitive).

Opaque Minerals

The unbrecciated eucrites contain chromite, ilmenite, troilite, and metal, although all four opaque minerals are not found in all eucrites. In general, abundant opaques tend to darken the overall spectrum (e.g., Johnson and Fanale 1973; Miyamoto et al. 1982; Cloutis et al. 1990). For example, Meteorite Hills (MET) 01081 and BTN 00300 have among the highest modal opaque mineral abundances (the combined abundance of chromite, ilmenite, troilite, and Fe-Ni metal) of the 11 unbrecciated eucrites and as a result exhibit lower absolute reflectance (Fig. 12). ALHA81001, a quench-textured eucrite, shows reduced spectral contrast relative to the other eucrites and yet does not contain a modally significant abundance of opaque minerals. Instead, the reduced spectral contrast of this sample can be attributed to micrometer-sized grains of ilmenite that are ubiquitous throughout the sample. If such spectra are observed on Vesta, then they may indicate similar quenched units on the surface

TESTING MODELS FOR THE PETROGENESIS OF VESTA

Having established that spectra can provide key insights into the crystallization and metamorphic history of basaltic terrains on Vesta, we can now examine whether these insights allow us to test the competing theories for how this diversity originated. The southern crater provides an ideal window into the crust of Vesta

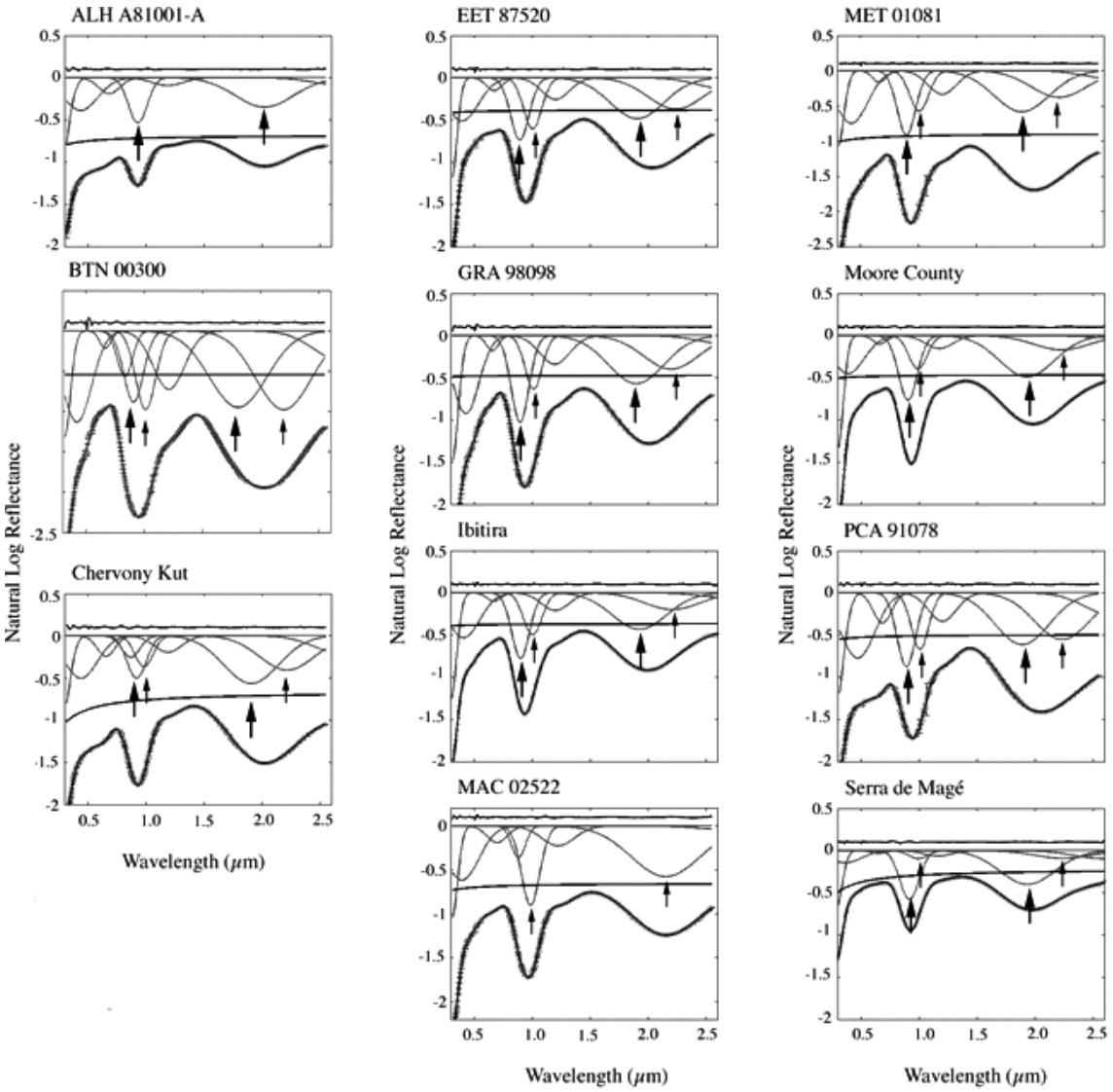

Fig. 9. MGM results for all eucrite spectra. Lines and symbols as given in Figs. 4 and 5. ALHA81001 and MAC 02522 are the only eucrites in this study that were fit using a one-pyroxene model. This can be seen in the 1 and 2 μm regions where only one band is present, in all other models there are two bands in each of these regions. MGM also allows variation in band strengths, band widths, and band center positions to be compared.

(Binzel et al. 1997; Gaffey 1997). The walls of the crater may allow mapping of units at depth and give a measure of their spatial extent. The central peak of the impact may have uplifted and exposed lower crustal lithologies on the surface of Vesta, and possibly even the upper mantle. Here, the predictions of the competing models for the petrogenesis of Vesta are outlined, then examined in terms of the spectral features and changes that would be expected for each one.

Magma Ocean

A global magma ocean should produce laterally extensive homogeneous lithologies. Spectral changes would likely be observed on a smaller scale vertically than horizontally. In the magma ocean model, the diogenites are envisaged to form by crystal accumulation (Ruzicka et al. 1997); intrusion of diogenite material into the eucritic crust should be limited if this model is correct and should instead form a separate layer beneath that of the eucrites. With depth a shift from basaltic eucrites to cumulate eucrites to diogenites is predicted. Such a shift should be observable in the spectra as the HCP content is decreasing with depth and this will be accompanied by both continuum-removed band center positions shifting toward shorter wavelengths, a decrease in the strength of the 1.2 μm M1 pyroxene band, and a change in the spectrally derived LCP:HCP ratio. Horizontally, along

Table 5. MGM results for unbrecciated eucrites.

	ALHA 81001	BTN 00300	Chervony Kut	EET 87520	GRA 98098	Ibitira	MAC 02522	MET 01081	Moore County	PCA 91078	Serra de Magé
Continuum-removed band centers (μm)											
Band 1	0.94	0.95	0.94	0.95	0.94	0.94	0.97	0.94	0.94	0.96	0.93
Band 2	2.01	2.01	2.01	2.02	2.01	2.00	2.13	2.00	1.99	2.02	1.97
MGM band centers (μm)											
Additional M1		0.83	0.87				0.88				
LCP at 1		0.91	0.92	0.90	0.90	0.90		0.90	0.91	0.89	0.92
HCP at 1	0.93	1.01	0.99	1.01	1.01	1.01	0.99	1.01	0.99	1.01	1.00
1.2 feature	1.19	1.21	1.19	1.20	1.20	1.20	1.12	1.21	1.18	1.20	1.17
LCP at 2		1.81	1.91	1.91	1.90	1.93		1.89	1.93	1.89	1.94
HCP at 2	2.02	2.20	2.22	2.24	2.12	2.21	2.15	2.22	2.23	2.24	2.24
MGM relative strengths (log reflectance)											
Additional M1		−0.56	−0.26				−0.36				
LCP at 1		−0.89	−0.51	−0.74	−1.03	−0.78		−0.92	−0.77	−0.88	−0.58
HCP at 1	−0.54	−0.98	−0.37	−0.61	−0.63	−0.50	−0.90	−0.58	−0.40	−0.67	−0.10
1.2 feature	−0.09	−0.73	−0.20	−0.26	−0.34	−0.21	−0.23	−0.34	−0.15	−0.34	−0.07
LCP at 2		−0.95	−0.57	−0.49	−0.57	−0.43		−0.59	−0.49	−0.62	−0.40
HCP at 2	−0.35	−0.98	−0.41	−0.37	−0.40	−0.20	−0.37	−0.38	−0.17	−0.56	−0.09
LCP/HCP at 1		0.91	1.37	1.22	1.62	1.57		1.59	1.93	1.31	6.03
LCP/HCP at 2		0.97	1.39	1.30	1.43	2.17		1.54	2.88	1.11	4.30
MGM band widths (μm)											
Extra M1							0.14				
LCP at 1	0.00	0.20	0.19	0.19	0.18	0.18		0.19	0.19	0.19	0.19
HCP at 1	0.19	0.20	0.18	0.18	0.17	0.18	0.19	0.19	0.18	0.18	0.19
1.2 feature	0.32	0.32	0.28	0.28	0.31	0.28	0.34	0.29	0.28	0.29	0.28
LCP at 2	0.00	0.58	0.56	0.55	0.57	0.56		0.56	0.56	0.55	0.56
HCP at 2	0.60	0.56	0.56	0.56	0.56	0.56	0.70	0.56	0.56	0.56	0.56

Note: MGM = modified Gaussian model; LCP = low-Ca pyroxene; HCP = high-Ca pyroxene.

the crater walls it may then be possible to map the spatial extent of each spectrally distinct unit.

Partial Melting and Serial Magmatism

While the widespread metamorphism seen in the eucrites supports the serial magmatism theory put forward by Yamaguchi et al. (1996), the history of Vesta's crust is, in reality, far more complex (Mayne et al. 2009). Partial melting would produce a layered crust on a much smaller scale relative to the magma ocean model. Different eucrite lava flows would be stacked up upon one another, producing lithologic, and therefore spectral, variation on a small scale both vertically and horizontally.

In this model, the cumulate eucrites are formed as later intrusions into the basaltic crust. This would be best tested by using MGM predicted LCP:HCP ratios, the depth of the 1.2 μm M1 pyroxene band, and the position of continuum-removed band centers as all of these are affected by changing HCP content. Cumulate eucrites (lower HCP content, shallower 1.2 μm band that is often not visually apparent, shorter continuum-removed band centers) would be seen to crosscut different basaltic eucrite layers with depth but be on a smaller lithologic scale horizontally.

Assessing Current Models for Vesta's Formation Using ALHA81001

ALHA81001 is a quench-textured eucrite that cooled quickly on its parent body. It contains Cr-rich pyroxenes, suggesting that it crystallized from a primitive magma. The fact that ALHA81001 retains some of the original compositional crystallization trends within its pyroxenes indicates that it did not experience the same high level of metamorphism so common within the eucrites as a whole. Any model put forward for the petrogenesis of Vesta must also be able to explain all the features seen within ALHA81001.

In a partial melting model, the suggested global metamorphism of the eucrites is explained by successive lava flows on the surface insulating those flows beneath, resulting in a slower cooling rate (e.g., Takeda and Graham 1991; Yamaguchi et al. 1996). The fact that ALHA81001 does not appear to have been affected by this is best explained by its formation late in Vesta's history, as one of the last melts to crystallize. Its

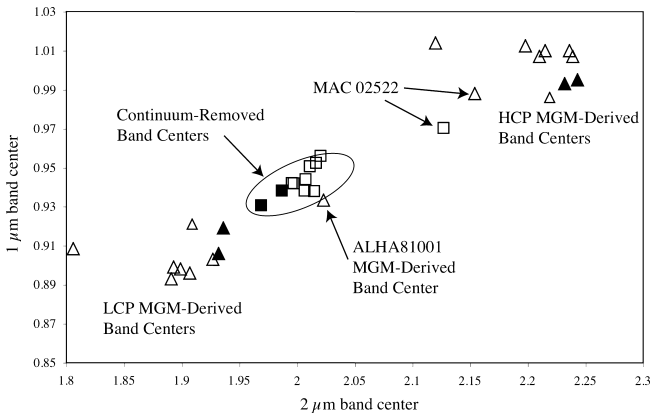

Fig. 10. Eucrite continuum-removed and MGM-derived band centers. The unbrecciated eucrite band centers divided into cumulate (filled symbols) and basaltic (open symbols). Continuum-removed values are shown as squares and triangles represent MGM-derived band centers. The cumulate eucrites have continuum-removed band centers at the shortest wavelengths due to their lower modal abundance of HCP. The MGM-derived band centers for the eucrite all cluster together, reflecting the similar major-element chemistry of both LCP and HCP within these meteorites. The continuum-removed band centers for MAC 02522 lie at much longer wavelengths than the other eucrites. This is most likely due to the high iron content of the pyroxene in MAC 02522 relative to the average of the other eucrite pyroxenes. MGM requires only one-pyroxene model to fit MAC 02522 and allows us to identify it as a zoned pyroxene from the anomalously wide bands used in the model (Sunshine and Pieters 1993). ALHA81001 also only required a one-pyroxene model and, therefore, does not have separate LCP and HCP MGM-derived band centers.

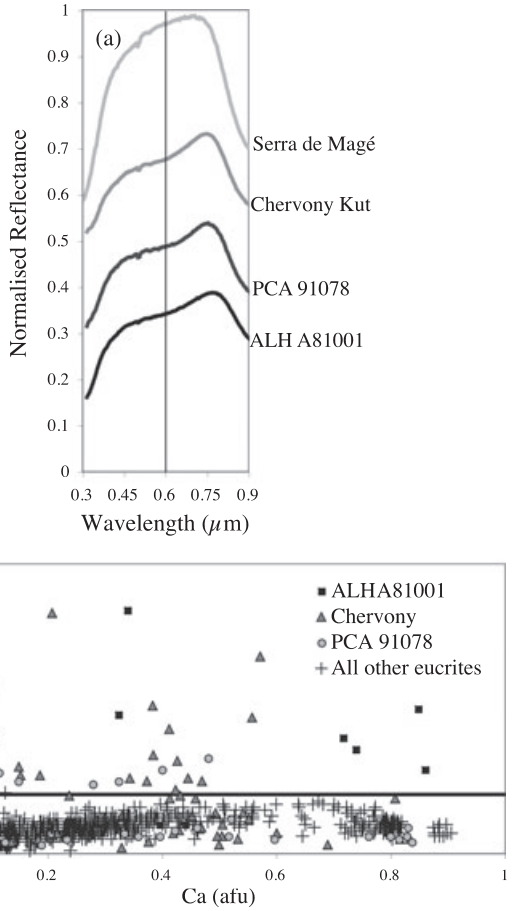

Fig. 11. Presence of the 0.6 μm Cr^{3+} feature in the spectra of the unbrecciated eucrites. a) Portion of VNIR spectra for the unbrecciated eucrites showing the 0.6 μm absorption. The Serra de Magé spectrum is illustrated as an example of a spectrum with no absorption visually present. b) Plot of Ca versus Cr in atomic formula units for the pyroxenes in the unbrecciated eucrites. Ca is used here for illustrative purposes and not to indicate some relationship between Cr and Ca content. The detection limit of Cr_2O_3 on the electron microprobe is around 0.03 wt%, which translates to 0.001–0.002 afu. All samples with a Cr-content >0.02 afu in their pyroxenes exhibit a visually obvious 0.6 μm absorption feature.

quenched nature means that it probably formed either on the surface or as the quench margin on an ascending late-stage partial melt from primitive mantle material that intruded into cold country rock. Recent work by Barrat et al. (2007) suggests such a late-stage partial melt origin for the Stannern trend eucrites.

It is much more difficult to envisage the formation of ALHA81001 in a magma ocean environment. Pyroxenes rich in compatibles, such as Cr, would have to crystallize out of the magma ocean early. This would explain the composition of ALHA81001, but it seems impossible for such early formed samples to then avoid being highly metamorphosed during the following stages of the magma ocean's history. One possible environment where a primitive (early formed), yet unmetamorphosed eucrite could form would be the quench crust, or convective lid of the magma ocean. This would mean that the entire surface of Vesta was initially covered with ALHA81001-like material, whereas the contrasting partial melting model predicts this only on a small scale. The paucity of eucrites similar to ALHA81001 could be used to argue for the latter model, but the true test is to look at Vesta itself.

We have shown here that rapidly cooled units with Cr-rich pyroxenes like ALHA81001 can be identified spectrally on the surface of Vesta by the presence of a visible 0.6 μm feature and their reduced spectral contrast, a result of widespread fine-grained opaque minerals formed during quenching. The extent to which a visible 0.6 μm feature is observed over Vesta's surface will be key to deciphering its formation history. Before Dawn arrives at Vesta this idea is being tested on the Vestoids, a group of asteroids believed to originate from Vesta (Mayne et al., in preparation). If a visible 0.6 μm feature is common in Vestoid spectra, then it is

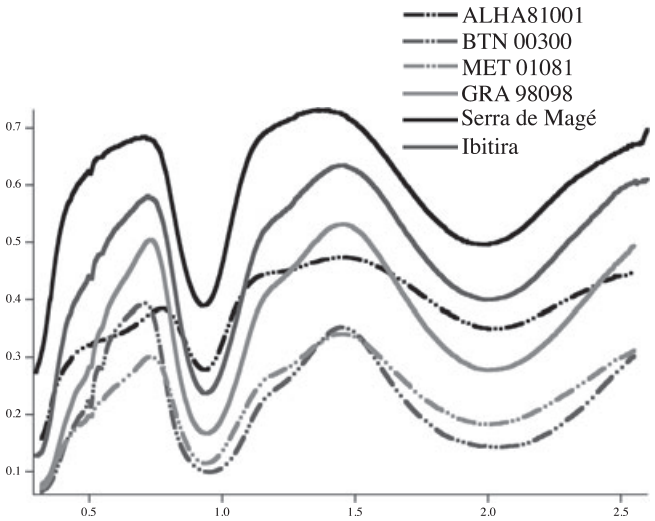

Fig. 12. VNIR reflectance spectra of six unbrecciated eucrites showing the difference in reflectance values and spectral contrast between samples. BTN 00300, MET 01081, and ALHA81001 (dotted lines) can be seen to have a lower spectral contrast than the other eucrites shown. BTN 00300 and MET 01081 are rich in opaque phases (chromite, ilmenite, sulfides, and metal), which are known to darken the overall spectrum (Johnson and Fanale 1973). However, the reduced contrast seen in ALHA81001 does not reflect a high modal abundance of opaques, instead this eucrite contains very fine-grained ilmenite scattered throughout the sample. This is a result of its fast-cooling rate.

reasonable to assume Cr-rich pyroxenes are abundant on the surface of Vesta itself.

CONCLUSIONS

In this study, we have investigated the relationship between the petrology and spectra of the unbrecciated eucrites, to determine how spectroscopy can be used as a tool to understand the petrogenesis of Vesta.

- The pyroxene chemistry of the eucrites dominates their spectra.
- A good estimate of the pyroxene modal mineralogy of the eucrites can be obtained from their spectra (i.e., LCP:HCP). However, no information regarding the abundance of plagioclase can be deduced from these spectra.
- A Cr-feature is visible at 0.6 μm. Cr-rich pyroxenes crystallized from primitive magmas, which may allow mapping of the evolution of units on the surface of Vesta.
- Most of the eucrites are metamorphosed and, as a result, have equilibrated mineral compositions. Those samples that preserve their Cr-rich pyroxenes did not experience the same high level of metamorphism and their identification on Vesta would aid in interpreting the thermal history of the surface.
- The models proposed for the formation of Vesta predict different crustal structures and lithologic variety on different scales. The data presented here have shown that these predictions can be tested using spectroscopy.
- The eucrite ALHA81001 is a Cr-rich, quench-textured, unmetamorphosed eucrite, which suggests that it crystallized close to, or on the surface of its parent body, but it was not affected by the metamorphism that affected the majority of the eucrites. This limits the possible environments in which ALHA81001 could have formed. It is hard to envisage the formation of ALHA81001 in the magma ocean model. ALHA81001 would have to represent the quench crust on the surface and it would be an abundant unit on the surface of Vesta. Conversely, if the partial melting model is correct then ALHA81001 could represent a late-stage primitive melt. Therefore, the geologic context of units akin to ALHA81001 on the surface of Vesta may prove key in determining which model best fits the observations of Dawn at Vesta.

Acknowledgments—This work was supported by PGG grant NNX06AH69G to J. M. S. and NASA Cosmochemistry grant NNG06GG36G and UCLA subcontract 2090-S-JB694 for Dawn to H. Y. M. All meteorite spectra were collected at Brown University's KECK/NASA Reflectance Experiment Laboratory (RELAB). Thanks go to M. Darby Dyar for the collection of Mössbauer spectra.

Editorial Handling—Dr. Beth Ellen Clark

REFERENCES

Adams J. B. 1974. Uniqueness of visible and near-infrared diffuse reflectance spectra of pyroxenes and other rock-forming minerals. *Journal of Geophysical Research* 79:4829–4836.

Adams J. B. 1975. Interpretation of visible and near-infrared diffuse reflectance spectra of pyroxenes and other rock-forming minerals. In *Infrared and Raman spectroscopy of lunar and terrestrial materials*, edited by Karr C. Jr. New York: Academic Press. pp. 91–116.

Adams J. B. and Goullaud L. H. 1978. Plagioclase feldspars: Visible and near infrared diffuse reflectance spectra as applied to remote sensing. Proceedings, 9th Lunar and Planetary Science Conference. pp. 2901–2909.

Adams J. B., Hörz F., and Gibbons R. V. 1979. Effects of shock-loading on the reflectance spectra of plagioclase, pyroxene, and glass (abstract). 30th Lunar and Planetary Science Conference. pp. 1–3.

Barrat J. A., Yamaguchi A., Greenwood R. C., Bohn M., Cotton J., Benoit M., and Franchi I. A. 2007. The Stannern trend eucrites: Contamination of main group

eucritic magmas by crustal partial melts. *Geochimica et Cosmochimica Acta* 71:4108–4124.
Binzel R. P. and Xu S. 1993. Chips off asteroid 4 Vesta: Evidence for the parent body of basaltic achondrite meteorites. *Science* 260:186–191.
Binzel R. P., Gaffey M. J., Thomas P. T., Zellner B. H., Storrs A. D., and Wells E. N. 1997. Geologic mapping of Vesta from 1994 Hubble Space Telescope images. *Icarus* 128:95–103.
Burns R. G. 1993. *Mineralogical applications of crystal field theory*, 2nd ed. New York: Cambridge University Press. 551 p.
Cloutis E. A. 2002. Pyroxene reflectance spectra: Minor absorption bands and effects of elemental substitutions. *Journal of Geophysical Research* 107:E6, doi:10.1029/2001/JE001590.
Cloutis E. A. and Gaffey M. J. 1991. Pyroxene spectroscopy revisited: Spectral-compositional correlations and relationship to geothermometry. *Journal of Geophysical Research* 96:22,809–22,826.
Cloutis E. A., Gaffey M. J., Smith D. G. W., and Lambert R. St. J. 1990. Reflectance spectra of mafic silicate-opaque assemblages with applications to meteorite spectra. *Icarus* 84:315–333.
Corrigan C. M., McCoy T. J., Sunshine J. M., Bus S. J., and Gale A. 2007. Does spectroscopy provide evidence for widespread partial melting of asteroids? I: Mafic mineral abundances (abstract #1463). 37th Lunar and Planetary Science Conference. CD-ROM.
Delaney J. S. and Prinz M. 1984. The polymict eucrites. *Journal of Geophysical Research* 89:C251–C288.
Gaffey M. J. 1976. Spectral reflectance characteristics of the meteorite classes. *Journal of Geophysical Research* 81:905–920.
Gaffey M. J. 1997. Surface lithologic heterogeneity of asteroid 4 Vesta. *Icarus* 127:130–157.
Gaffey M. J., Bell J. F., Brown R. H., Burbine T. H., Piatek J. L., Reed K. L., and Chaky D. A. 1993. Mineralogic variations within the S-type asteroid class. *Icarus* 106:573–602.
Gooding J. L. 1981. Mineralogic changes during terrestrial weathering of Antarctic chondrites. Proceedings, 12th Lunar and Planetary Science Conference. pp. 1105–1122.
Hardersen P. S., Gaffey M. J., and Abell P. A. 2004. Mineralogy of asteroid 1459 Magnya and implications for its origin. *Icarus* 167:170–177.
Harvey R. P. and McSween H. Y. 1992. The petrogenesis of the nakhlites: Evidence from cumulate mineral zoning. *Geochimica et Cosmochimica Acta* 56:1655–1663.
Hiroi T., Pieters C. M., Vilas F., Sasaki S., Hamabe Y., and Kurahashi E. 2001. The mystery of 506.5 nm feature of reflectance spectra of Vesta and Vestoids: Evidence for space weathering? *Earth, Planets and Space* 53:1071–1075.
Jarosewich E., Nelen J., and Norberg J. 1979. Electron microprobe reference samples for mineral analysis. *Smithsonian Institution Contributions to the Earth Sciences* 22:68–72.
John C. M. 2004. Plotting and analyzing data trends in ternary diagrams made easy. *EOS Transactions American Geophysical Union* 85(16), doi:10.1029/2004EO160004.
Johnson T. V. and Fanale F. P. 1973. Optical properties of carbonaceous chondrites and their relationship to asteroids. *Journal of Geophysical Research* 78:8507–8518.
Kanner L. C., Mustard J. F., and Gendrin A. 2007. Assessing the limits of the Modified Gaussian Modal for remote spectroscopic studies of pyroxenes on Mars. *Icarus* 187:442–456.
Klima R. L., Pieters C. M., and Dyar M. D. 2007. Spectroscopy of synthetic Mg-Fe pyroxenes I: Spin-allowed and spin-forbidden crystal field bands in the visible and near-infrared. *Meteoritics & Planetary Science* 42:235–253.
Klima R. L., Pieters C. M., and Dyar M. D. 2008. Characterization of the 1.2 μm M1 pyroxene band: Extracting cooling history from near-IR spectra of pyroxenes and pyroxene-dominated rocks. *Meteoritics & Planetary Science* 43:1591–1604.
Lazzaro D., Michtchenko T., Carvano J. M., Binzel R. P., Bus S. J., Burbine T. H., Mothe-Diniz T., Florczak M., Angeli C. A., and Harris A. W. 2000. Discovery of a basaltic asteroid in the outer main belt. *Science* 288:2033–2035.
Mason B. 1962. *Meteorites*. New York: J. Wiley and Sons.
Mayne R. G., McSween H. Y., McCoy T. J., and Gale A. 2009. Petrology of the unbrecciated eucrites. *Geochimica et Cosmochimica Acta* 73:794–819.
McCord T. B., Adams J. B., and Johnson T. V. 1970. Asteroid Vesta: Spectral reflectivity and compositional implications. *Science* 168:1445–1447.
McCoy T. J., Corrigan C. M., Sunshine J. M., Bus S. J., and Gale A. 2007. Does spectroscopy provide evidence for widespread partial melting of asteroids? II: Pyroxene compositions (abstract #1631). 37th Lunar and Planetary Science Conference. CD-ROM.
McCoy T. J., Mittlefehldt D. W., and Wilson L. 2006. Asteroid differentiation. In *Meteorites and the early solar system II*, edited by Lauretta D. S. and McSween H. Y. Jr. Tucson, AZ: The University of Arizona Press. pp. 733–746.
McFadden L. A. and McCord M. J. 1978. Prospecting for plagioclase on Vesta. *Bulletin of the American Astronomical Society* 10:601.
McSween H. Y. and Treiman A. H. 1998. Martian meteorites. In *Planetary materials*, edited by Papike J. J. Reviews in Mineralogy, vol. 36. Washington, D.C.: Mineralogical Society of America. pp. 6:1–53.
Mittlefehldt D. W. 1994. The genesis of diogenites and HED parent body petrogenesis. *Geochimica et Cosmochimica Acta* 58:1537–1552.
Mittlefehldt D. W. and Lee M. T. 2001. Petrology and geochemistry of unusual eucrite GRA 98098 (abstract). *Meteoritics & Planetary Science* 36:A136.
Mittlefehldt D. W. and Lindstrom M. M. 2003. Geochemistry of basaltic eucrites, and Hf and Ta as petrogenetic indicators for altered Antarctic eucrites. *Geochimica et Cosmochimica Acta* 67:1911–1935.
Miyamoto M., Mito A., and Takano Y. 1982. An attempt to reduce the effects of black materials from the spectral reflectance of meteorites and asteroids. *Memoirs of the National Institute of Polar Research Special Issue* 20:345–361.
Mustard J. F. 1992. Chemical analysis of actinolite from reflectance spectra. *American Mineralogist* 77:345–358.
Palme H. and Rammensee W. 1981. The significance of W in planetary differentiation processes: Evidence from new data on eucrites. Proceedings, 12th Lunar and Planetary Science Conference. pp. 949–964.

Pieters C. M. 1983. Strength of mineral absorption features in the transmitted component of near-infrared reflected light: First results from RELAB. *Journal of Geophysical Research* 88:9534–9544.

Pieters C. M. and Hiroi T. 2004. RELAB (Reflectance Experiment Laboratory): A NASA multi-user spectroscopy facility (abstract #1720). 35th Lunar and Planetary Science Conference. CD-ROM.

Pieters C. M., Binzel R. P., Bogard D., Hiroi T., Mittlefehldt D. W., Nyquist L., Rivkin A., and Takeda H. 2005. Asteroid-meteorite links: The Vesta conundrum(s). *Asteroids, Comets, Meteors Proceedings, IAU Symposium* 229:273–288.

Pun A. and Papike J. J. 1996. Unequilibrated eucrites and the equilibrated Juvinas eucrite: Pyroxene REE systematics and major, minor, and trace element zoning. *American Mineralogist* 81:1438–1451.

Righter K. and Drake M. J. 1997. A magma ocean on Vesta: Core formation and petrogenesis of eucrites and diogenites. *Meteoritics & Planetary Science* 32:929–944.

Rossman G. R. 1980. Pyroxene spectroscopy. In *Pyroxenes*, edited by Prewitt C. Reviews of Mineralogy, vol. 7. Washington, D.C.: Mineralogical Society of America. pp. 95–115.

Russell C. T., Coradini A., Christensen U., De Sanctis M. C., Feldman W. C., Jaumann R., Keller H. U., Konopliv A., McCord T. B., McFadden L. A., McSween H. Y., Mottola S., Neukum G., Pieters C. M., Prettyman T. H., Raymond C. A., Smith D. E., Sykes M. V., Williams B., Wise J., and Zuber M. T. 2004. Dawn: A journey in space and time. *Planetary and Space Science* 52:465–489.

Russell C. T., Capaccioni F., Coradini A., Christensen U., De Sanctis M. C., Feldman W. C., Jaumann R., Keller H. U., Konopliv A., McCord T. B., McFadden L. A., McSween H. Y., Mottola S., Neukum G., Pieters C. M., Prettyman T. H., Raymond C. A., Smith D. E., Sykes M. V., Williams B., and Zuber M. T. 2006. Dawn discovery mission to Vesta and Ceres: Present status. *Advances in Space Research* 38:2043–2048.

Ruzicka A., Synder G. A., and Taylor L. A. 1997. Vesta as the howardite, eucrite, and diogenite parent body: Implications for the size of a core and for large-scale differentiation. *Meteoritics & Planetary Science* 32:825–840.

Salisbury J. W. and Hunt G. R. 1974. Meteorite spectra and weathering. *Journal of Geophysical Research* 79:4439–4441.

Schade U. and Wäsch R. 1999. Near-infrared reflectance spectra from bulk samples of the two SNC meteorites Zagami and Nakhla. *Meteoritics & Planetary Science* 34:417–424.

Stolper E. 1977. Experimental petrology of eucritic meteorites. *Geochimica et Cosmochimica Acta* 41:587–611.

Sunshine J. M. and Pieters C. M. 1993. Estimating modal abundances from the spectra of natural and laboratory pyroxene mixtures using the Modified Gaussian Model. *Journal of Geophysical Research* 98:9075–9087.

Sunshine J. M., Pieters C. M., and Pratt S. F. 1990. Deconvolution of mineral absorption bands: An improved approach. *Journal of Geophysical Research* 95:6955–6966.

Sunshine J. M., McFadden L. A., and Pieters C. M. 1993. Reflectance spectra of the Elephant Moraine A79001 meteorite: Implications for remote sensing of planetary bodies. *Icarus* 105:79–91.

Sunshine J. M., Bishop J., Dyar M. D., Hiroi T., Klima R., and Pieters C. M. 2004a. Near-infrared spectra of Martian pyroxene separates: First results from Mars Spectroscopy Consortium (abstract #1636). 35th Lunar and Planetary Science Conference. CD-ROM.

Sunshine J. M., Bus S. J., McCoy T. J., Burbine T. H., Corrigan C. M., and Binzel R. P. 2004b. High-calcium pyroxene as an indicator of differentiation in asteroids and meteorites. *Meteoritics & Planetary Science* 39:1343–1357.

Takeda H. and Graham A. L. 1991. Degree of equilibration of eucritic pyroxenes and thermal metamorphism of the earliest planetary crust. *Meteoritics* 26:129–134.

Treiman A. L. 1990. Complex petrogenesis of the Nakhla (SNC) meteorite: Evidence from petrography and mineral chemistry. Proceedings, 20th Lunar and Planetary Science Conference. pp. 273–280.

Yamaguchi A., Taylor G. J., and Keil K. 1996. Global crustal metamorphism of the eucrite parent body. *Icarus* 124: 97–112.